Available online at www.sciencedirect.com
SCIENCE DIRECT®
Journal of Molecular Catalysis A: Chemical 233 (2005) 111–120
JOURNAL OF MOLECULAR CATALYSIS A: CHEMICAL
www.elsevier.com/locate/molcata

Catalysis and characterization of a rugged lead ruthenate pyrochlore membrane catalyst

Jyh-Harng Ke, Annamalai Senthil Kumar, Jun-Wei Sue, Shanmuganathan Venkatesan, Jyh-Myng Zen*

Department of Chemistry, National Chung Hsing University, 250 Kuo Kuang Road, Taichung 402, Taiwan

Received 9 August 2004; received in revised form 31 January 2005; accepted 1 February 2005

Abstract

A rugged lead ruthenate pyrochlore (Py, $Pb_2Ru_2O_6O'$) Nafion® 417 membrane catalyst (|NPy|) has been prepared by an in situ precipitation method and characterized by physico-chemical techniques. The Nafion® 417 membrane enhanced the Py crystallization to form a stable and continuous agglomerate-like structure in the |NPy| network. The cationic exchange characteristics of Nafion® 417 membrane was not fully suppressed after Py modification. Catalytic performance was demonstrated for the one pot and selective oxidation of benzyl alcohol to benzaldehyde via a perruthenate (RuO_4^-) intermediate with 30% H_2O_2 (as a sacrificial co-oxidant) in a triphasic condition (i.e. CH_2Cl_2/NPy/H_2O_2). Four repeated experiments with the |NPy| entailed a weight loss of ∼0.07% with virtually the same catalytic performance. With these inherent features, this membrane catalyst is useful in diverse research fields including organic synthesis, fuel cells, charge storage systems, etc.

Keywords: Nafion® 417; Lead ruthenate pyrochlore; Catalyst; Benzyl alcohol oxidation

1. Introduction

Lead ruthenate pyrochlore (Py, $Pb_2Ru_2O_6O'$) has been reported as an active catalyst for fuel cells, organic syntheses, charge storage capacitors and chemical sensors [1–9]. Since the Py catalyst possesses tunable oxidation states with interstitial oxygen vacancies, it is bi-functional for oxygen evolution reaction (OER), carbohydrate oxidations, oxygen reduction reaction (ORR), etc. [1,5,6,9–11]. Incorporation/modification of such a unique catalytic unit into a macromolecular heterogeneous structure of Nafion® membrane certainly holds advantages in various applications. Nafion® (a perfluorinated ionomeric membrane, Scheme 1) is a promising and stable host for the technological applications like fuel cells. Normally, a catalytic layer is mechanically/chemically modified on one side for faradic reaction and the other side of membrane is involved in reverse faradic reaction coupled with proton conductivity [12,13]. Nafion®/catalyst composites together with suitably designed electrochemical cells have been used in electroorganic synthesis [14–17].

Our group previously reported a Nafion®/Py chemically modified electrode (NPyCME), in which Nafion® solution is spin-coated on electrode surface followed by in situ precipitation of Py units directly inside the internal structure [8–10]. Such a modified electrochemical system served as good amperometric sensors for various analytical applications with a lifetime of more than 3 months. By adopting the preparation route, we further developed a macro Nafion® membrane/Py system that proved very useful for organic synthesis. Very recently we disclosed our green chemistry approach regarding a Py-modified $Ru(bpy)_3^{2+}$-doped multicomponent Nafion® membrane (5 cm × 5 cm) system (designated as |NPy–$Ru(bpy)_3^{2+}$|) for photocatalytic oxidation of organic sulfur-containing molecules to sulfoxide [18]. The Nafion®/Py membrane (designated as |NPy|) was extraordinarily stable in nonaqueous medium (immersed in 99% ethanol for up to 3 months at room temperature) [18]. In or-

* Corresponding author. Tel.: +886 4 2285 4007; fax: +886 4 2286 2547.
E-mail address: jmzen@dragon.nchu.edu.tw (J.-M. Zen).

1381-1169/$ – see front matter © 2005 Elsevier B.V. All rights reserved.
doi:10.1016/j.molcata.2005.02.008

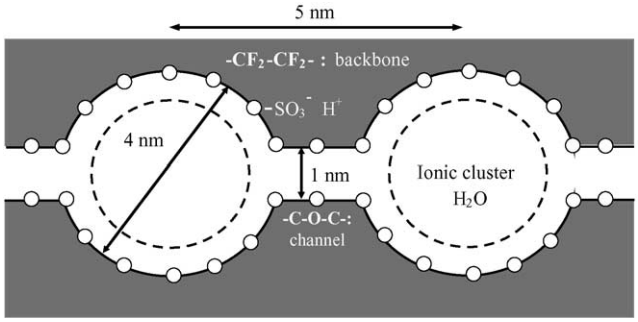

Scheme 1. Structure of the perfluorinated ionomer membrane (Nafion®).

der to understand the nature and characteristics of the |NPy| composite films, the fundamental aspects of the |NPy| catalyst was studied in this report. Selective oxidation of benzyl alcohol to benzaldehyde was further demonstrated as a catalytic model to express the |NPy| performance. The present approach is under a heterogeneous tri-phase catalytic condition without any electrochemical setup and thus differs from regular Nafion®-electrochemical systems used for synthetic electroorganic applications [14–17]. To the best of our knowledge, this is the first report on the use of membrane/catalyst composite directly for organic synthesis.

Selective synthesis of benzaldehyde from benzyl alcohol without any over-oxidation to benzoic acid is a key technological process that requires challenging synthetic routes [19]. Conventional procedures were directed towards stoichiometric and homogenous phase oxidations using environmentally toxic metals (like chromium), and often require complicated experimental conditions to achieve the desired selectivity [20–22]. Ruthenium-based composites, such as $RuCl_3{\cdot}xH_2O/H_2O_2$, perruthenate-zeolite, zeolite confined nano-RuO_2/air, hydroxyapatite-containing monomeric Ru/air, derivatives of Ru-oxo and/or -hydroxo complexes/tert-butyl hydroperoxide (TBHP), and Ru–Al_2O_3/air, were reported for the alcohol oxidation [19,23–29]. However, 100% product selectivity and reusability were not common. In addition, procedures of recovering the powder catalyst samples were too cumbersome. Since the |NPy| catalyst used here is in the macroscopic size (~1 cm^2); just a laboratory tong is enough to immediately recover it from the reaction mixture. The article covers detailed preparation, physico-chemical characteristics and catalytic response of the |NPy| catalyst towards organic synthesis.

2. Experimental

2.1. Materials and reagents

$RuCl_3{\cdot}xH_2O$, $Pb(NO_3)$, $[Ru(bpy)_3]Cl_2$, ferrocene, methanol, and Nafion® 417 (perfluorinated membrane reinforced with Teflon® and Dacron®, 0.017 in. thickness) were purchased from Aldrich and used as received. All the other compounds and organic solvents were of spectrophotometric grade and used without further purification. Aqueous solutions were prepared with doubly distilled deionized water.

2.2. Apparatus and measurements

X-ray diffraction (XRD, Shimadzu XRD-6000) measurements were carried out using a Cu Kα (1.54060 Å) radiation source. Other instruments used here are a scanning electron microscope (SEM, Oxford), an atomic force microscope (AFM, SPI 3800 Series), a solid-state UV–vis spectroscope (Labguide, Taiwan), a thermo-gravimetric apparatus (TGA, Seiko SSC 5200 at a scan rate of 10 °C/min), a scanning electrochemical microscope (SECM, CH instruments), and a gas liquid chromatograph (GLC, China chromatography 9800, Taiwan). GLC measurements were all carried out using a homemade stainless steel column containing 10% SP-2100 on a Chromosorb W HP (80/100 mesh) support. The optimized GLC temperature conditions are; injection = 200 °C, FID = 200 °C and the oven was kept at 150 °C for 4 min, then the temperature was increased at a rate of 10 °C/min to 250 °C as a final temperature for 5 min. A 5-μL sample injection volume was used without any loop.

The SECM instrumentation has been described in detail elsewhere [30,31]. The electrochemical system consists of a 10 μm Pt-ultramicroelectrode (UME) with Ag/AgCl (3 M KCl) as the reference and Pt as the counter electrodes. The unmodified and Py modified Nafion® membranes were carefully mounted on a homemade plastic plate on the bottom of the SECM cell. The top position of the cell was covered with 1 mM ferrocenemethanol (E° = 0.31 V versus SCE) in 0.2 M KCl. The distance of the UME was set by carefully positioning the tip (*z*-axis), while simultaneously measuring the transport limited current (i_{tlc}) of ferrocenemethanol ($Fc^{+/0}$) redox system. The tip was maneuvered in the *z*-axis from an infinite distance to the working membrane surface at which the i_{tlc} approached 20% of the original value (usually ~90% is acceptable for smooth surfaces [30]). However since the membrane surface is unsmooth (via SEM), relatively low current values and high interface distances were chosen here. Images of the transport-limited current versus tip position were obtained by scanning at 1.5 μm/s in a fixed plane above the working membrane surface.

2.3. In situ precipitation of Py into Nafion® 417 membrane

Scheme 2 shows the typical preparation route for the |NPy| catalyst [18]. Briefly, a piece of Nafion® 417 membrane with a geometric area of ~10 cm^2 was first ion-exchanged overnight in 31.8 mM Ru^{3+} + 47.6 mM Pb^{2+} 100 mL solution followed by thorough washing with deionized water to remove the cations not ion-exchanged. Then the modified membrane was submersed in 1.1 M KOH at 53 °C for 24 h with constant O_2 purging. The preparation procedure resulted in a uniform distribution of the catalytically active micro-

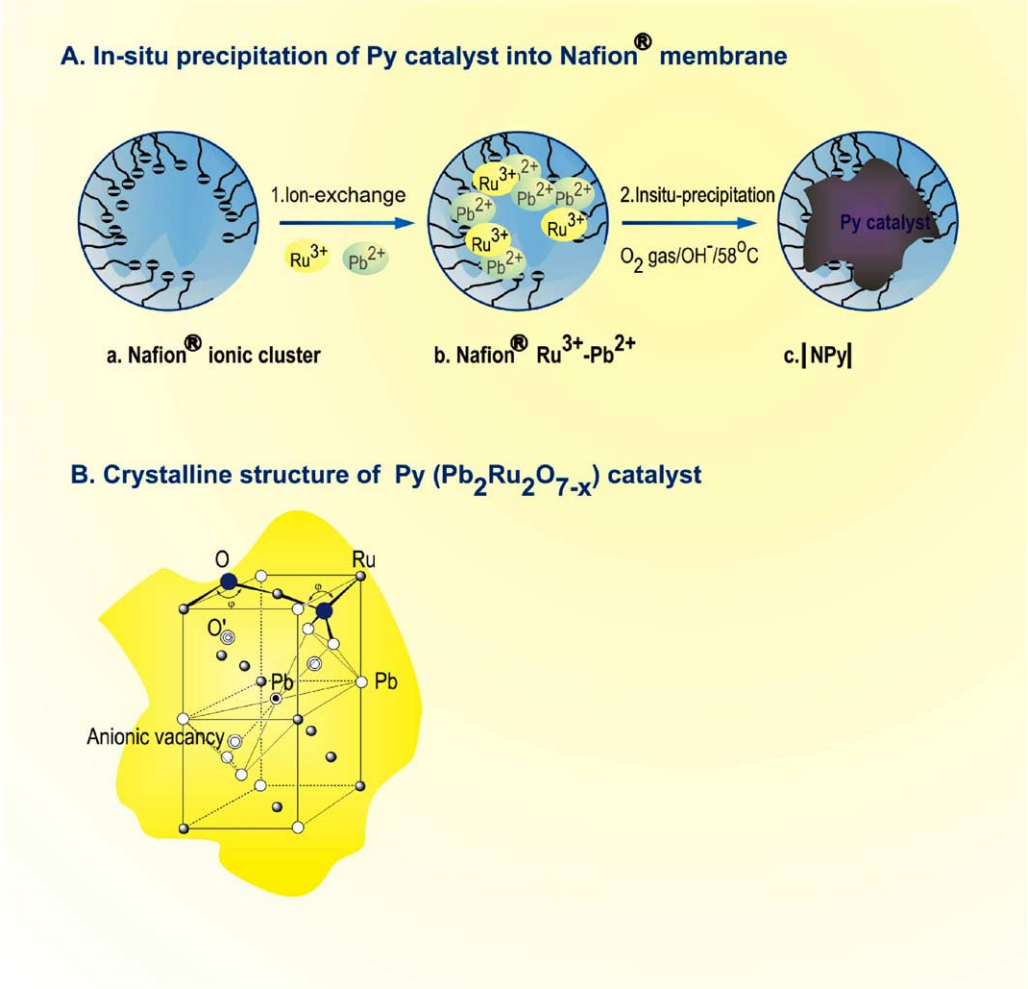

Scheme 2. (A) Preparation route of the |NPy|. (B) Crystalline structure of the active Py site.

particles throughout the Nafion® 417 membrane matrix as confirmed by SEM. The weight difference of Nafion® 417 membrane before and after Py modification was calculated at ~0.06 g/g (i.e. 70.6 μmol of Py units per gram of membrane). The formation of Py inside the Nafion® film was confirmed through XRD patterns in the latter section.

2.4. General procedure for selective benzyl alcohol oxidation reaction

Benzyl alcohol (50 μL, ~32 mM) was first dissolved in 15 mL CH_2Cl_2 under constant stirring with ~1 g of |NPy| membrane catalyst (~1 cm^2). The reaction temperature was set at 80 °C with the slow addition of 30% H_2O_2 (total volume either 3 or 9 mL). The |NPy| catalyst requires higher H_2O_2 initially. Reaction rates were continuously monitored by analyzing the non-aqueous layer during the course of reaction with GLC. After a prescribed reaction time, the catalyst was removed by using laboratory tongs and then the product was simply separated via evaporation of the non-aqueous layer by using a rotary evaporator. Relative GLC peak areas with respect to its standards were uniformly taken as quantitative parameters for the percentage conversion calculation. The catalytic activity of the membrane was regenerated by washing in sequence with copious amount of $CH_2Cl_2 \rightarrow CH_3–CO–CH_3 \rightarrow H_2O \rightarrow$ 1.1 M KOH (with stirring at least for 1 h) $\rightarrow H_2O$ and then dried at 50 °C for 3 h.

3. Results and discussion

3.1. Physico-chemical characteristics of the |NPy| catalyst

3.1.1. XRD measurements

Fig. 1 shows the comparative X-ray diffraction patterns of the Nafion® 417 membrane, Py powder, and Nafion/Py composite membrane. As can be seen, the Py powder shows a broad XRD 2θ peak centered at 30° and another diffuse wave in the window of 40–60°. On the other hand, the |NPy| composite membranes prepared under similar conditions show

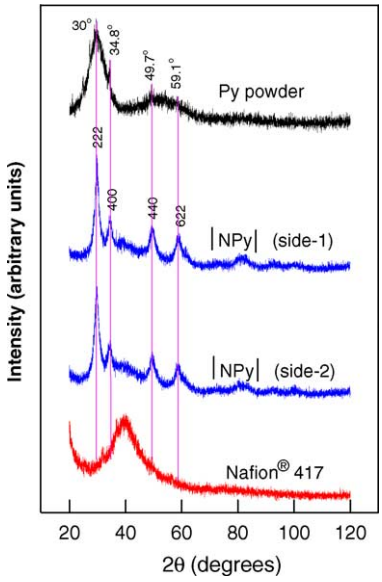

Fig. 1. X-ray diffraction patterns of the |NPy| catalyst (both sides) in comparison with unmodified Py powder and Nafion® 417 membrane samples.

sharp peaks at 30, 34.8, 49.7 and 59.1° (in agreement with the standard values of the Py crystalline powder) [9,32]. The XRD peaks of |NPy| were relatively sharper than those of bare Py powder. The results indicate an enhancement in the crystallinity of Py in the |NPy| composite membrane. In other words, the Nafion® membrane can assist the crystallization of Py in Nafion® interfacial structures.

In XRD powder diffraction patterns, peak broadening can be related to three different factors: i.e. strain, faulting, and grain size [33,34]. The strain and faulting can be easily predicted by observing the 2θ-peak shift. Since the major peak at $2\theta = 30^\circ$ is virtually the same for all three cases, the possibility of strains and faulting were thus ruled out. The grain size change causes the peak broadening. The grain size (t, nm) of the Py particles can be calculated from the broadening of XRD peak using the Scherrer formula below [33]:

$$t = \frac{0.9\lambda}{B\cos\theta} \quad (1)$$

where λ is the source of the X-ray wavelength (0.154 nm), B is the full width of the half maximum (FWHM) value (in radians) and θ is the diffraction angle. The $2\theta = 30^\circ$ peak was taken uniformly for the "t" assignment. An FWHM value of 1.35° was calculated for the |NPy|. For the case of Py powder, the coupled response was first deconvoluted into 30° (FWHM = 3.85°) and 34.8° (FWHM = 0.2°), respectively, using a homemade Gaussian model [35], and then the 30° peak is further chosen for the "t" calculation. Based on Eq. (1), the "t" values were calculated at 1.4 and 5.3 nm, respectively, for the Py powder and |NPy| membrane samples. The crystalline grain size of Py in |NPy| was ~4 times as large as that of the unmodified Py powder. Such an obvious alteration is related to the structural factor of the membrane.

The Nafion® network can be visualized as a reverse micelle-like ionic cluster (4 nm diameter) with three distinctive structural regions, i.e. perfluorinated backbone polymer network (hydrophobic zone, $-CF_2-CF_2-$), water cores (hydrophilic area, $-SO_3^-X^+ \cdot nH_2O$), and an interfacial domain (where water cores in neighboring clusters are interconnected through 1 nm channels, –C–O–C–) (Scheme 1) [36–38]. Note that the Py grain size of 5.3 nm for the composite membrane is slightly higher over the cluster size of Nafion® membrane (4 nm). Liu et al. observed a particle size of 3.8 nm for Nafion®-composite membrane with TiO_2 [39]. In another case, Ludvigsson et al. observed a grain size of 30 nm for the composite of MnO_2 and Mn_2O_3 with Nafion® by XRD and the possible structure was not explored [40]. Presumably, the grains might grow over the clusters with an agglomerate like network structure for the case of large grain size system in the Nafion®. Regarding the enhanced XRD peaks with the|NPy|, the close packing of Pb^{2+} and Ru^{3+} ions in the cluster sites of Nafion® should aid in the increased crystallinity of the Py. Further studies with SEM, AFM, SECM, and TGA reveal important structural factors about the |NPy| membrane.

3.1.2. SEM analysis

Fig. 2 shows SEM images and energy dispersive X-ray analysis (EDAX) of the |NPy| catalyst. As can be seen, a pancake type of morphology without any marked cracks in the surface was observed. Surface morphology is quite different in different sides. For example, a pancake type of morphology can be seen in the top side, while the bottom position shows a smooth and folded-wire like surface (may be due to the membrane net, cross-section SEM in Fig. 2D and E). Presumably, the top position was relatively rough and more hydrophilic in nature. There is no obvious difference in the XRD for those sides, further reminiscent of similar Py crystallize units throughout the |NPy| structure (Fig. 1). There is no appearance of isolated Py particles in the |NPy| in accordance to the value of 5.3 nm by XRD and unlike the case of the TiO_2 modified Nafion® membrane [39].

The nature of the Nafion® backbone and preparation conditions should consequently affect the critical morphological structure of the composite membrane. For example, Nafion® composite prepared at high temperatures and/or with strong chemical treatments (such as light paraffin and Pd-alloy modified films sputtered at 300 and 100 °C, respectively [41,42]) leads to more surface cracks. While mild treatments (such as ion-exchange followed by hot water hydrolysis [39]) result in uniform distribution without any surface cracks as is the case of TiO_2. Classical preparation procedures utilize Nafion® 117 as a host and the surface structures can be easily influenced by external modification procedures [39-42]. Considering that Nafion® 417 used in this work possesses a more rigid network due to reinforced Teflon® and Decron® polymeric units, it is rugged enough to protect the network from surface cracks even in harsh environments. Hence, the catalyst having rigid structure is free

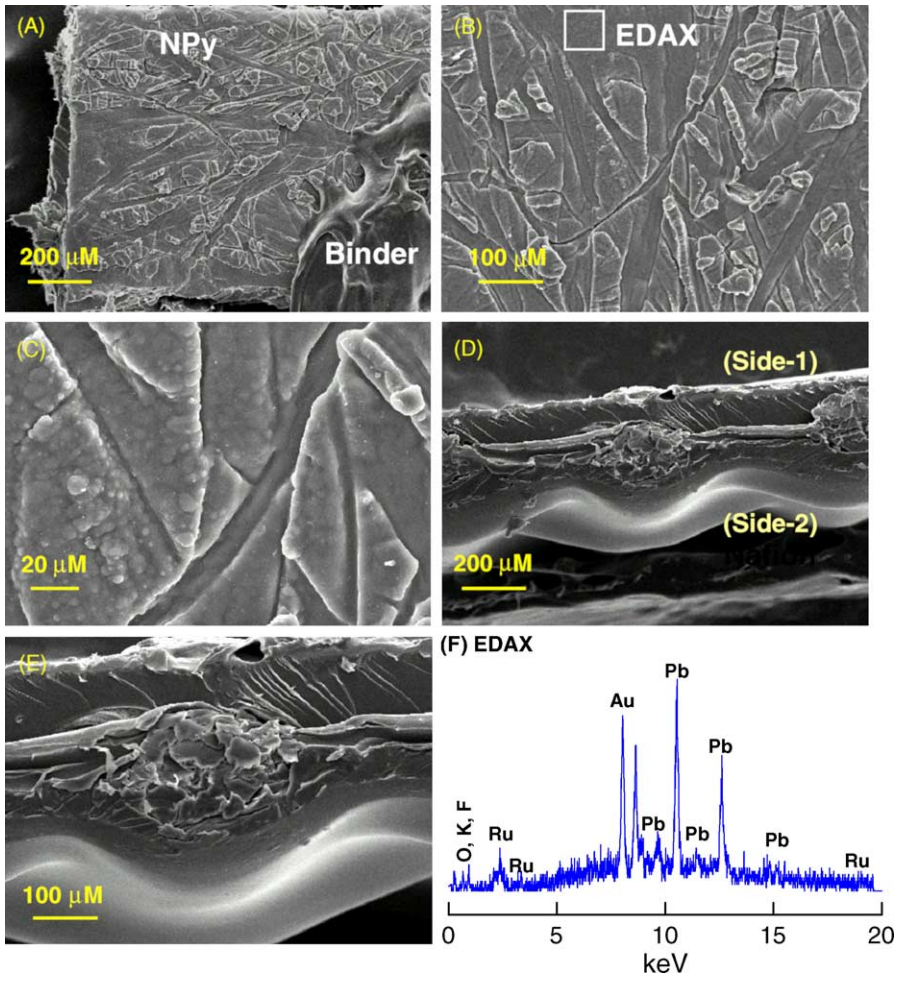

Fig. 2. SEM of the |NPy| membrane (Au coated) at different magnifications and its typical EDAX response.

from any surface cracks and is faithfully useful for synthetic applications.

3.1.3. AFM analysis

Fig. 3 shows the typical surface morphology for the |NPy| membrane. Even though the general structure result is close to that of SEM analysis, the AFM results reveal a fine surface structure with mild contours on the networks. The top view AFM reveals agglomerate-like structures with various size nano-particles. An average particle size of ~30 nm was detected in remote places (Fig. 3B), which is 7.5 times as large as the Nafion® ion-cluster size and in consistent with the XRD observation. The larger particle size observed by AFM are agglomerated units of the 5.3 nm Py particles. In other words, the observation provides a clue about the number of grains in the agglomerated units. For example, ~6 numbers of the 5.3 nm Py particles were clubbed together to make the ~30 nm size agglomerate in the |NPy| network. The inter-cluster Py formation dominated in |NPy| further diminishes the individual intra-Py particles. Again, continuous distribution of the Py catalytic sides throughout the Nafion® membrane is apparent.

3.1.4. SECM analysis

SECM is a useful electrochemical technique for imaging the surface topographical structure at solid/liquid interfaces [30,31,43,44]. A negative feedback mode was adopted here, where the diffusion/transport current of the Mh-$Fc^{+/0}$ redox system is hindered by the membrane contours. In turn the transport-limited current, i_{tlc}, at a fixed applied potential (0.3 V versus Ag/AgCl) can be monitored as a surface topological structure (Fig. 4A).

Typical three-dimensional SECM image of the bare Nafion® 417 and |NPy| using Pt-UME over a 50 μm × 50 μm area is shown in Fig. 4. The |NPy| film shows relatively higher contour levels over the bare Nafion® 417 membrane, presumably due to the Py modified layer and there are no other obvious differences. Note that the surface topology viewed by SECM is the in situ permeable regions of the underlying surface and this result further reflect that the Py anchored Nafion® 417 membrane has sufficient active-layers in the |NPy|'s surface for catalytic applications. Overall, the SECM observation is in parallel with the SEM and AFM morphological views regarding the continuous distribution of Py catalytic sites in the |NPy| catalyst.

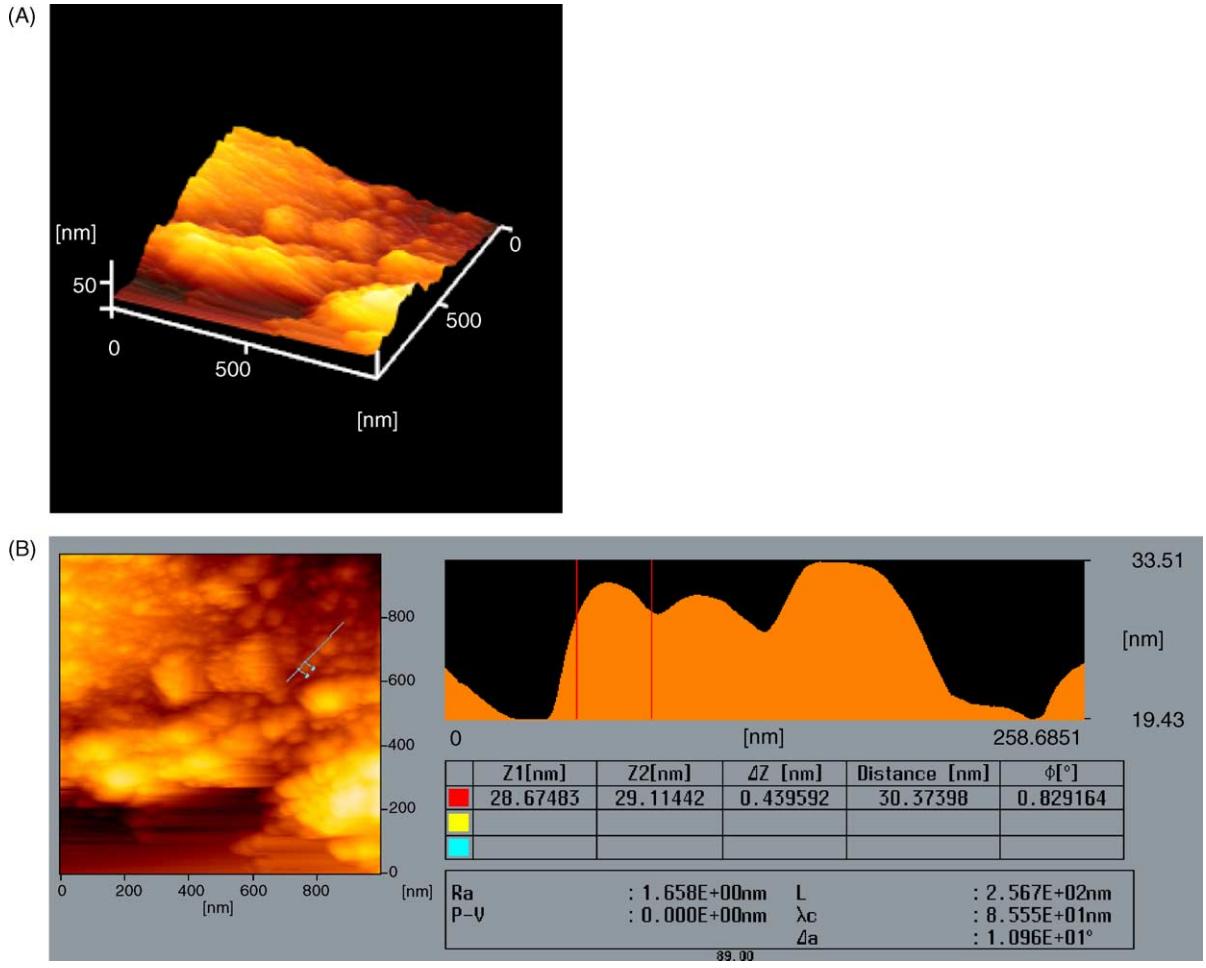

Fig. 3. AFM surface morphology view of the |NPy| catalyst (side-1) (A) and in-built program result for the calculation of particle size on the surface (B).

3.1.5. TGA studies

Fig. 5 shows the thermal decomposition and its differential (DTGA) patterns of the Py powder, |NPy| and bare Nafion® 417 membrane in the temperature window of 30–900 °C. The Py powder shows feeble weight loss peaks at ∼100 and 300 °C, respectively, due to physisorbed, $(H_2O)_{phy}$ and chemisorbed, $(H_2O)_{chem}$ water or –OH, $(–OH)_{chem}$ molecules and the Py powder is fairly stable up to 800 °C. While the |NPy| maintains its weight up to 400 °C without any marked weight-loss, but at >400 °C it starts to lose its weights due to the degradation of $–SO_3^-$, –C–O–C– (400–500 °C) and $–CF_2–$ (500–600 °C) functional groups [38,45]. This is qualitatively similar to the case of bare Nafion® 417 membrane (Fig. 5c and Scheme 3). The observation is also true with Nafion® 117 membrane except at increased temperatures [45]. The reinforced nature and rigid structure of Nafion® 417 cause the shift of the degradation temperature. Fig. 5B shows the comparative TGA at extreme temperatures (500–700 °C). Interestingly the bare Nafion® 417 resulted in a 100% weight loss, while the |NPy| retained ∼9% weight at 800 °C. The remaining amount in the latter case is closer to the calculated weight of ∼6% for the Py particles inside the |NPy| from the initial weight-loss measurements. Scheme 3 shows possible thermal degradation pathways for the |NPy| based on the TGA data. At extreme temperature (>600 °C) the Nafion® units were completely burned out and leaving the nude Py powder in the test system. But, at $T < 400$ °C, the

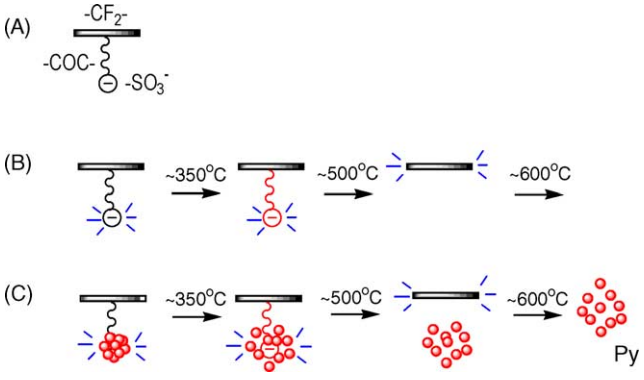

Scheme 3. Conceptional representations for the decomposition pathways of the Nafion® 417 (A and B) and |NPy|units (C) under thermogravimetric analysis. Lighter colors denote partial decomposition of the compounds.

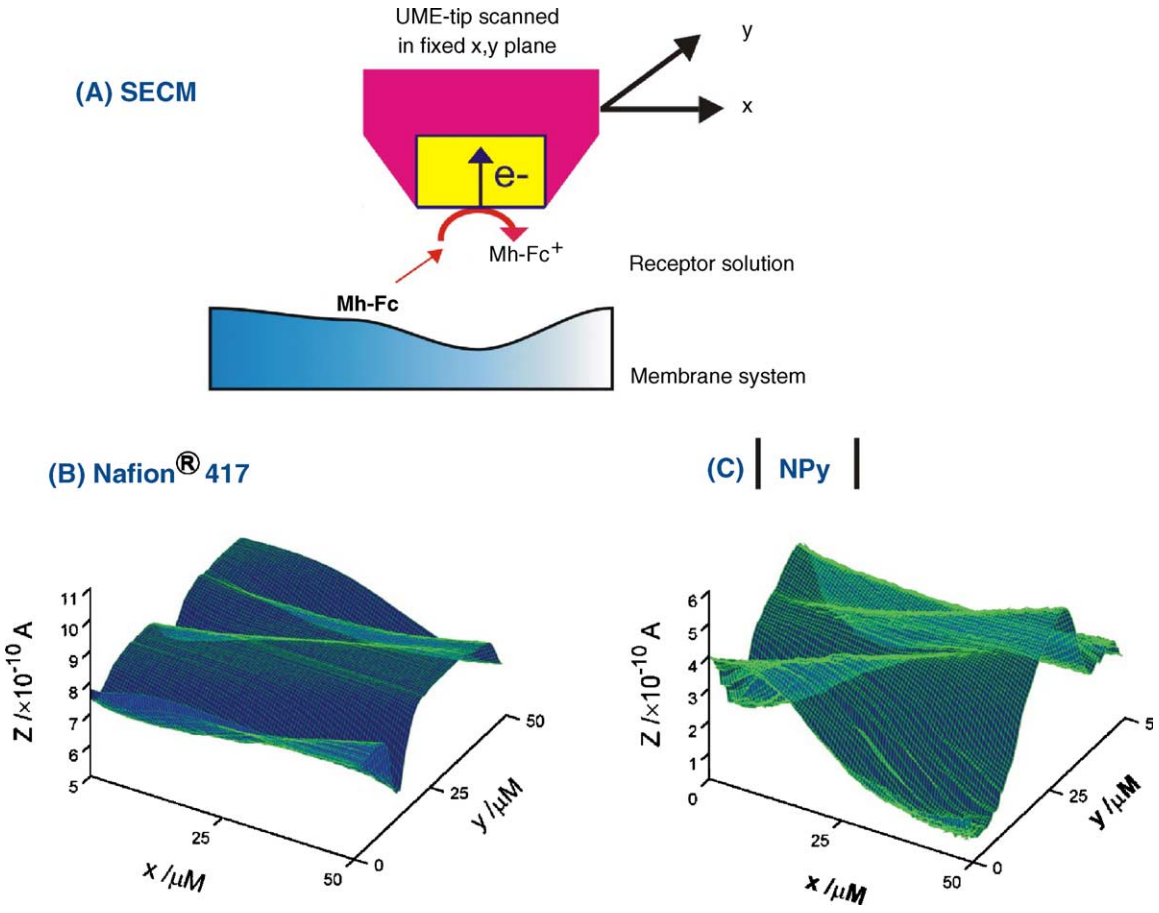

Fig. 4. Schematic illustration for the SECM operation using a Pt UMP tip (A), and the topographical images for the bare Nafion® 417 (B) and |NPy| composite membrane (C) (side-1) (the scales *x* and *y* = distance, *z* = current).

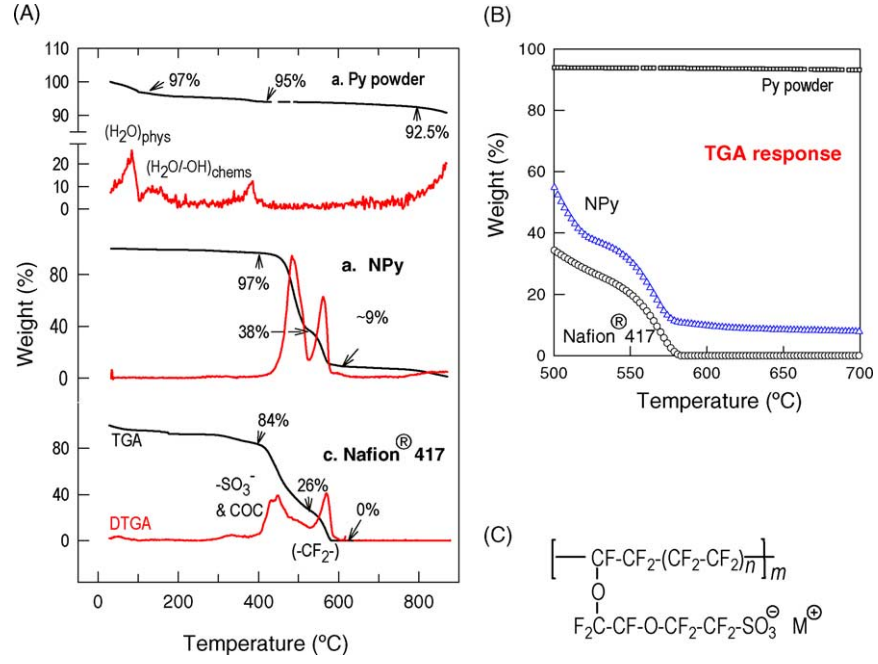

Fig. 5. Typical TGA and DTGA response for the |NPy| catalytic system in comparison to the bare Py and Nafion® 417 samples in the temperature window of 30–900 °C (A), 500–700 °C (B) and basic chemical structure for the Nafion® (C).

membrane achieve is rigid and stable and is thus suitable for use in hot-bath catalytic synthesis.

3.1.6. Cation exchange property (CEP)

Since the Nafion® membrane is prone to cationic exchange behavior, the ion-exchange ability of the membrane after the Py modification was studied. The photosensitizer, $Ru(bpy)_3^{2+}$, is taken as a probe to analyze the CEP using its specific λ_{max} band at 456 nm. If the Py catalyst is completely loaded or blocked on the Nafion® membrane, there is no free anionic sulfonic group, which will result in failure in $Ru(bpy)_3^{2+}$ ion-exchange and thus the absence of any absorption signal. On the other hand, if the Py is partially loaded with considerable exposure of the free anionic sulfonic groups, then obvious absorption signals can be observed corresponding to the ion-exchanged $Ru(bpy)_3^{2+}$ into the |NPy| composite. Fig. 6 shows typical solid-state UV–vis absorption spectra of the bare |NPy| and $Ru(bpy)_3^{2+}$ composite films treated at ambient conditions. It is obvious that the thick opaque |NPy| membrane resulted in a highly noisy behavior, while the $Ru(bpy)_3^{2+}$ treated membrane showed a specific peak at about 450 nm corresponding to the $Ru(bpy)_3^{2+}$ absorption energy level. This observation is partially reminiscent of the Py formation and the cationic exchangeable vacancies in the |NPy| composite system.

3.2. Selective benzyl alcohol oxidation reaction

Catalytic oxidation reactions were typically carried out in a three-necked round bottom flask with 32.8 mM of benzyl alcohol in 15 mL CH_2Cl_2 at 80 °C. The |NPy| catalyst (~1 g) was placed in the flask and the co-oxidant (30% H_2O_2) was slowly added (0.5 mL h^{-1}). Reaction rates were continuously

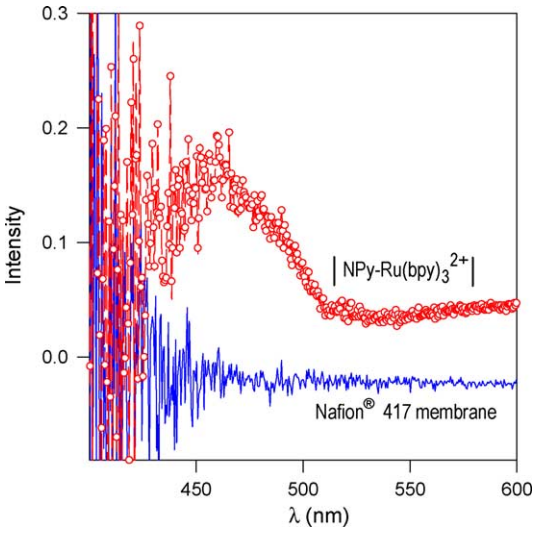

Fig. 6. Solid state UV–vis absorption spectrum of Nafion® 417 and $Ru(bpy)_3^{2+}$-modified |NPy| catalytic system (|NPy–$Ru(bpy)_3^{2+}$|) in ambient conditions. In the modification procedure, 1 cm^2 test membrane is first dipped in 1 mM $Ru(bpy)_3^{2+}$ CH_3CN:H_2O (1:1) solution for ~30 min followed by water washing.

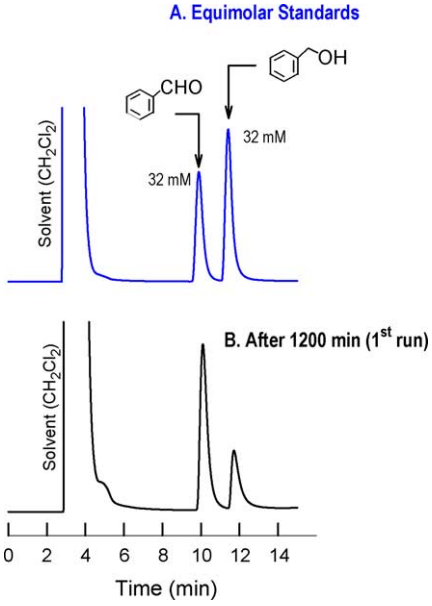

Fig. 7. Typical GLC response for the equimolar standards of benzyl alcohol and benzaldehyde (A) and from the |NPy| catalyzed benzyl alcohol reaction mixture (B) under optimized GLC conditions.

monitored by analyzing the non-aqueous layer during the course of reaction with GLC. Fig. 7 shows the GLC data for the 50:50 molar ratio of both benzyl alcohol and benzaldehyde standards under optimized GLC working conditions (A) and the typical response (1200 min) from the fresh reaction mixture (B) with ~80% conversion of benzaldehyde. Parallel oxidation experiments in the absence of catalyst and with low 30% H_2O_2 amount (3 mL) did not show any appreciable conversion with very poor yield (Table 1). This result reveals the necessity of the catalytic system with the addition of considerable co-oxidant. Based on the GLC results, the catalytic kinetic rate constant (k_{cat}) for the psuedo first order benzyl alcohol oxidation was calculated as shown in Table 1. The k_{cat} value was in the range of $2–3.6 \times 10^{-6}$ s^{-1} for the catalytic oxidation, while it is about two order higher than that of the uncatalyzed reaction. Measured turnover frequency (TOF) for the catalyst was in the range of 16–23 h^{-1}, which is in close agreement with values in the range of 3–28 h^{-1} for the zeolite-confined nano-RuO_2 powder system [25]. Extended product analysis experiments using GLC–MS, H^1 NMR and C^{13} NMR shows benzaldehyde and some trace of starting material (data not included). Note that the $RuCl_3 \cdot xH_2O$ based classical system yielded both benzaldehyde and benzoic acid products [23]. Hence, the observation with the |NPy| based catalytic system allows 100% benzaldehyde selectivity without any over-oxidation to benzoic acid.

As to the mechanism, the high valent perruthenate/ruthenate, $Ru^{VII}O_4^-/Ru^{VI}O_4^{2-}$ redox couple exists in the |NPy| surface is believed to participate in the benzyl alcohol oxidation with the H_2O_2 as per the reaction (Scheme 4). In the first step, the co-oxidant H_2O_2 helps to convert the ruthenate (RuO_4^{2-}) to high-valent perruthenate ion (RuO_4^-) in aque-

Table 1
Selective catalytic oxidation of $PhCH_2OH \rightarrow PhCHO$ using |NPy| catalyst in CH_2Cl_2 + 30% H_2O_2 at 80 °C

Catalyst entry	$PhCH_2OH$ (mM)	|NPy| (g)		H_2O_2 (mL)[d]	Time (h)	Yield[c] (%)	k_{cat}[a] ($\times 10^{-5}$) (s^{-1})	TOF[b] (h^{-1})
		Added	Recovered					
Blank	32	–	–	9	24	6.3	0.06	–
|NPy| (fresh)	32	1.026	1.019	9	24	84.0	2.03	16
|NPy| (second time)	32	1.019	1.019	9	20	99.0	3.59	23
|NPy| (third time)	32	1.019	1.017	3	6	16.0	1.19	16
|NPy| (fourth time)	32	1.017	1.012	9	24	89.1	2.38	17

[a] First order rate constant.
[b] Turn over frequency (TOF) = $[product]_{Mol}/([catalyst]_{Mol} \times T_{hour})$; [Py] = 70.56 μmol/g of NPy.
[c] By GLC.
[d] Slow addition in the reaction mixture (condition not optimized).

ous solution, which in turn oxidizes the benzyl alcohol to benzaldehyde (organic phase) and return to the low-valent RuO_4^{2-} in a cyclic manner (Scheme 4). Electrogeneration of the perruthenate intermediate ion is the key for the benzyl alcohol oxidation, which is usually stabilized in alkaline condition or organic solvents [46]. In the above reaction scheme, H_2O_2 acted as a sacrificial electron acceptor for the overall oxidation. It is expected that fraction of basic cationic sites exist in the |NPy| achieve helps for the easy abstraction of proton from the $PhCH_2OH$ (β-hydride elimination reaction pathway similar to ≻Ru=O based metal complex for the alcohol oxidation) [47] in turn to the selective benzaldehyde formation and the behavior is yet to be studied in detail. Further steps towards the acceleration of the reaction rate using solution pH, H_2O_2 flow rate and interphase-assisting system (i.e. phase-transfer catalyst) are in progress.

Finally, the benzyl alcohol oxidation reaction was repeated several times under similar working conditions to evaluate the multiple re-usage of the |NPy| (Table 1). Fig. 8 shows the typical results for four repeated usages of the |NPy| catalyst. The conversion rates and yields were similar in all experiments revealing appreciable stability and reusability of the present system. Apart from this, easy separation of the |NPy| from the reaction mixture is another clear advantage of the present approach (Fig. 8C). Most importantly, ∼100% recovery of the catalytic system was observed. In short, even at stringent working conditions like 100 h of total reaction timings (T = 80 °C) with a strong stirring, a weight loss ∼0.07% only was noticed with the |NPy| catalyst. It is very difficult to expect such stable recoveries and reusability from conventional powder based catalytic systems, since the unknown quantities of waste in each step (like separation and cleaning) leads to considerable leakage of the active-catalyst from its matrix. Finally, the alcohol oxidation reaction is cleaner and environmentally nontoxic final products result in a "green" approach for further applications.

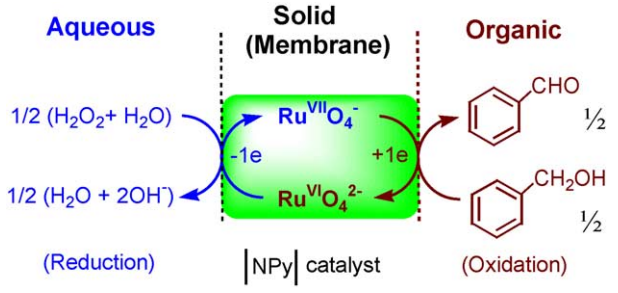

Scheme 4. Proposed triphasic benzyl alcohol oxidation mechanism on the |NPy| catalyst with 30% H_2O_2.

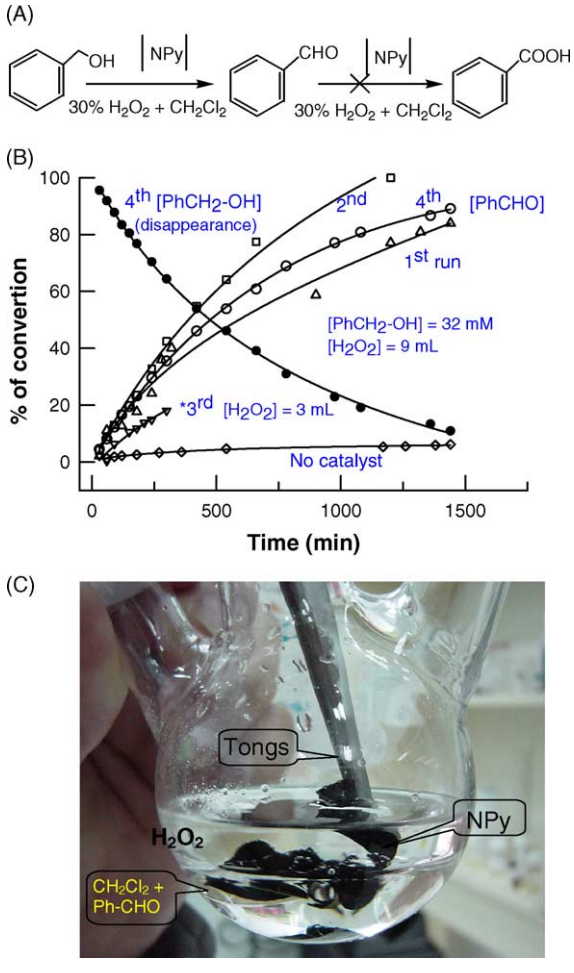

Fig. 8. (A) Reaction scheme for the selective benzyl alcohol oxidation without any over-oxidation to benzoic acid. (B) Plot of % of conversion over the reaction time for the benzyl alcohol oxidation reaction catalyzed by |NPy| at various recyclic conditions with 30% H_2O_2. (C) The reaction step up picture.

4. Conclusions

A rugged lead ruthenate pyrochlore (Py) catalyst-incorporated Nafion® 417 membrane (|NPy|) was thoroughly characterized with XRD, SEM, AFM, SECM, TGA, UV–vis absorption spectroscopic methods. XRD results reveal ∼3 times enhanced Py crystalline formation inside the Nafion® 417 membrane over the unmodified Py powder samples. The measured Py grain size of 5.3 nm (by XRD) for the |NPy| is slightly larger than the Nafion® cluster size of 4 nm. Surface morphological analysis shows a pancake like agglomerate structure of the |NPy| with the active Py catalyst mainly exposed in the outer surface and hence it is quite suitable for catalytic applications. Solid state UV–vis absorption spectroscopy study reveals the availability of free sulfonic acid sites even after the incorporation of Py in Nafion®. A practical catalytic application was demonstrated with ∼100% selective benzyl alcohol oxidation to benzaldehyde without any over oxidation to benzoic acid. The catalytic membrane was 100% recovered from the reaction mixture without any marked loss of the Py activity even after four continuous runs. Since the catalytic system possesses excellent stability, recovery, and repeatability over classical techniques, practical applications in organic synthesis, fuel cells, capacitors, etc., is anticipated. Further work is in progress in this direction.

Acknowledgments

The authors gratefully acknowledge the financial support from the National Science Council of Republic of China. We also thank Ting-Wei He and Prof. Hong-Yi Tang for technical supports.

References

[1] J.B. Goodenough, R. Manoharan, M. Paranthaman, J. Am. Chem. Soc. 112 (1990) 2076.
[2] J.-M. Zen, R. Manoharan, J.B. Goodenough, J. Appl. Electrochem. 22 (1992) 140.
[3] T. Takeda, R. Kanno, Y. Kawamoto, Y. Takeda, O. Yamamoto, J. Electrochem. Soc. 147 (2000) 1730.
[4] T.R. Felthouse, J. Am. Chem. Soc. 109 (1987) 7566.
[5] T.R. Felthouse, U.S. Patent 1990. Ser. No. 807,010.
[6] S.J.H.F. Arts, F. Van Rantwijk, R.A.J. Sheldon, Carbohyd. Chem. 15 (1996) 15.
[7] H.J. Bang, W.C. Lu, P.J. Fei, Electrochem. Comm. 2 (2000) 653.
[8] J.-M. Zen, A.S. Kumar, J.-C. Chen, Anal. Chem. 73 (2001) 1169.
[9] J.-M. Zen, A.S. Kumar, Acc. Chem. Res. 34 (2001) 772.
[10] J.-M. Zen, A.S. Kumar, J.-C. Chen, J. Mol. Catal. A 165 (2001) 177.
[11] J. Prakash, D.A. Tryk, E.B. Yeager, J. Electrochem. Soc. 146 (1999) 4145.
[12] A.S. Aricò, S. Srinivasan, V. Antonucci, Fuel Cells 1 (2001) 133.
[13] L. Carrette, K.A. Friedrich, U. Stimming, Fuel Cells 1 (2001) 5.
[14] J.-H. Jian, B.-L. Wu, C.-S. Cha, J. Electroanal. Chem. 417 (1996) 89.
[15] J.-H. Jian, B.-L. Wu, C.-S. Cha, Y.-Q. Zhou, J. Electroanal. Chem. 420 (1997) 31.
[16] O. Simond, Ch. Comninellis, Electrochim. Acta 42 (1997) 2013.
[17] D. Hoormann, C. Kubon, J. Jörissen, L. Kröner, H. Pütter, J. Electroanal. Chem. 507 (2001) 215.
[18] J.-M. Zen, S.-L. Liou, A.S. Kumar, M.-S. Hsia, Angew. Chem. Int. Ed. 42 (2003), 577 and 1328.
[19] M. Hudlický, Oxidations in Organic Chemistry. ACS Monograph 186, American Chemical Society, Washington, DC, 1990.
[20] Y.S. Rao, R. Filler, J. Org. Chem. 39 (1974) 3304.
[21] D. Dey, M.K. Mahanti, J. Org. Chem. 55 (1990) 5848.
[22] J. Muzart, A.N. Ajjou, S. Ait-Mohand, Tetrahedron Lett. 35 (1994) 1989.
[23] G. Barak, J. Dakka, Y. Sasson, J. Org. Chem. 53 (1988) 3553.
[24] D.L. Wu, A.P. Wight, M.E. Davis, Chem. Commun. (2003) 758.
[25] B.-Z. Zhan, M.A. White, T.-K. Sham, J.A. Pinock, R.J. Doucet, K.V.R. Rao, K.N. Robertson, T.S. Cameron, J. Am. Chem. Soc. 125 (2003) 2195.
[26] K. Yamaguchi, K. Mori, T. Mizugaki, K. Ebitani, K. Kaneda, J. Am. Chem. Soc. 122 (2000) 7144.
[27] C.-M. Che, K.-W. Cheng, M.C.W. Chan, T.-C. Lau, C.-K. Mak, J. Org. Chem. 65 (2000) 7996.
[28] W.-H. Cheng, W.-Y. Yu, W.-P. Yip, N.-Y. Zhu, C.-M. Che, J. Org. Chem. 67 (2002) 7716.
[29] K. Yamaguchi, N. Mizuno, Angew. Chem. Int. Ed. 41 (2002) 5438.
[30] A.J. Bard, M.V. Mirkin (Eds.), Scanning Electrochemical Microscopy, Marcel Dekker, New York, 2001.
[31] J.V. Macpherson, M.A. Beeston, P.R. Unwin, Langmuir 11 (1995) 3959.
[32] H.S. Horowitz, J.M. Longo, H.H. Horowitz, J.T. Lewandowski, in: R.K. Graselli, J.F. Brazdil (Eds.). Solid State Chemistry in Catalysis, ACS Symposium Series 279, ACS, Washington, DC, 1985, 143.
[33] B.D. Cullity, Elements of X-ray Diffraction, second ed., 1978.
[34] B.E. Warren, Diffraction by Imperfect Crystals, Dover Publication, New York, 1969, 251.
[35] A.S. Kumar, J.-M. Zen, Electroanalysis 16 (2004) 242.
[36] C. Heitner-Wirguin, J. Membr. Sci. 120 (1996) 1.
[37] T.D. Gierke, W.Y. Hsu, Macromolecules 15 (1982) 101.
[38] Y. Wang, Y. Kawano, S.R. Aubuchon, R. Palmer, Macromolecules 36 (2003) 1138.
[39] P. Liu, J. Bandara, Y. Lin, D. Elgin, L.F. Allard, Y.-P. Sun, Langmuir 18 (2002) 10398.
[40] M. Ludvigsson, J. Lindgren, J. Tegenfeld, J. Mater. Chem. 11 (2001) 1269.
[41] F. Frusteri, F. Arena, S. Bellitto, A. Parmaliana, Appl. Catal. A 180 (1999) 180.
[42] Z.Q. Ma, P. Cheng, T.S. Zhao, J. Membr. Sci. 215 (2003) 327.
[43] J. Kwak, A.J. Bard, Anal. Chem. 61 (1989) 1221.
[44] A.J. Bard, F.F.-R. Fan, D. Pierce, P.R. Unwin, D.O. Wipf, F. Zhou, Science 1991, 254, 68.
[45] S.K. Tiwari, S.K. Nema, Y.K. Agarwal, Thermochim. Acta 317 (1998) 175.
[46] A.S. Kumar, J.-M. Zen, Chem. Phys. Chem. 5 (2004) 1227.
[47] M.S. Thompson, T.J. Meyer, J. Am. Chem. Soc. 102 (1980) 2310.